

Article

Mediterranean Water Properties at the Eastern Limit of the North Atlantic Subtropical Gyre since 1981

Helena C. Frazão ^{*}  and Joanna J. Waniek 

Leibniz Institute for Baltic Sea Research Warnemünde, Seestraße 15, 18119 Rostock, Germany; joanna.waniek@io-warnemuende.de

* Correspondence: helena.frazao@io-warnemuende.de

Abstract: A high-quality hydrographic CTD and Argo float data was used to study the property changes along the westward branch of the Mediterranean Outflow Water (MOW) in the northeast Atlantic between 1981 and 2018. In this period, the temperature and salinity are marked by periods of cooling/freshening and warming/salinification. Since 1981, the MOW properties at the core decreased by -0.015 ± 0.07 °C year⁻¹ and -0.003 ± 0.002 year⁻¹. The different phases of the North Atlantic Oscillation (NAO) influence the main propagation pathways of the MOW into the North Atlantic basin, thus affecting the trends determined within different NAO-phases. The temperature and salinity show a strong correlation with NAO, with NAO leading the properties by 8 and 7 years, respectively, indicating a delayed response of the ocean to different forcing conditions. A decrease in oxygen concentration (-0.426 ± 0.276 μmol kg⁻¹ year⁻¹) was calculated for the same period; however, no connection with the NAO was found.

Keywords: Mediterranean Outflow Water; North Atlantic Oscillation; Northeast Atlantic; time-series



Citation: Frazão, H.C.; Waniek, J.J. Mediterranean Water Properties at the Eastern Limit of the North Atlantic Subtropical Gyre since 1981. *Oceans* **2021**, *2*, 266–280. <https://doi.org/10.3390/oceans2010016>

Academic Editor: Michael W. Lomas

Received: 18 December 2020

Accepted: 9 March 2021

Published: 15 March 2021

Publisher's Note: MDPI stays neutral with regard to jurisdictional claims in published maps and institutional affiliations.



Copyright: © 2021 by the authors. Licensee MDPI, Basel, Switzerland. This article is an open access article distributed under the terms and conditions of the Creative Commons Attribution (CC BY) license (<https://creativecommons.org/licenses/by/4.0/>).

1. Introduction

The Mediterranean Water flows out of the Strait of Gibraltar and mixes with the surrounding North Atlantic Central Water in the Gulf of Cadiz to form the Mediterranean Outflow Water (MOW). MOW is a high-salinity and warm water mass that enters the Gulf of Cadiz and sinks until it reaches a buoyant depth around 1000 dbar [1,2]. To the west of the Gulf of Cadiz, MOW spreads into the North Atlantic by two main advective-diffusive pathways (Figure 1a): northward, as an eastern boundary undercurrent following the western margin of the Iberian Peninsula into the western European continental slope [3,4] and westward, into the subtropical Northeast Atlantic [5,6]. MOW also spreads south-westward, mainly through the influence of Mediterranean Water lenses formed in the proximity of Cape St. Vicent [7], also known as Meddies [8–11]. Although the north- and westward pathways contribute more to the spreading of MOW into the North Atlantic than the southwestern branch [12], its flow along the Gulf of Cadiz is guided by the local topography [13] and influenced by tides [14]. A more detailed description of the complex outflow and its spreading dynamics can be found, for example, in Figure 10 of de Pascual-Collar [15].

As an anomalously warm and saline water mass at intermediate depths, MOW is an important source of salt and heat in the eastern North Atlantic [1]. Reid [3] showed that the penetration of Mediterranean Water into higher latitudes, mainly Nordic Seas, a critical region in the context of the global overturning circulation, might impact the deep water formation in the Northeast Atlantic, and ultimately alter the thermohaline circulation [16].

The water column in the North Atlantic down to 2000 m has been warming since the second half of the last century [17]. Until the 1980s, most studies showed warming at intermediate depths [18,19]. However, after the 1980s, the warming along the western branch reported so far by Potter & Lozier [19] reversed to cooling [20] and, during the last decade (2002–2010), no significant trend was found [21]. In contrast, the MOW along the

northward flow continued to warm until 2001 [22] and showed cooling and freshening afterwards until 2013 [23].

The variability of MOW's temperature and salinity in the Northeast Atlantic (NEA) has been attributed to (i) changes in the properties of the outflow waters [19,20,24] and (ii) basin-wide circulation changes that alter the preferential pathways of the MOW after exiting the Strait of Gibraltar [25–27]. Lozier & Sindlinger [25] showed that changes in the source waters have little impact on interannual to decadal property variations observed at the MOW. However, Chaudhuri et al. [27] and Bozec et al. [26] pointed out that changes in the preferential pathways of MOW can be attributed to the observed properties changes, despite the warming of the Mediterranean Outflow reported in some studies [28,29].

The North Atlantic Oscillation (NAO), as the primary mode of atmospheric variability in the North Atlantic, is connected to changes in properties and transports on different time scales, even at depths of intermediate waters [28,30]. The influence of NAO on the main pathways of MOW was identified by Bozec et al. [26] and Chaudhuri et al. [27], with a particular focus on the penetration of Mediterranean Waters into the subpolar gyre [25,31].

In this study, a dataset comprising hydrographic data and Argo float data was used to assess the variability of the MOW's properties at the core (1000–1100 dbar) in the northeastern border of the subtropical gyre between 1981 and 2018 (Figure 1a). First, we analyzed the scales of temporal changes in MOW properties in the core over 38 years. Second, the changes observed in the in situ time-series were compared with a global gridded product (EN4) [32]. Finally, we investigated the NAO's influence on the variability of the temperature and salinity at the MOW core.

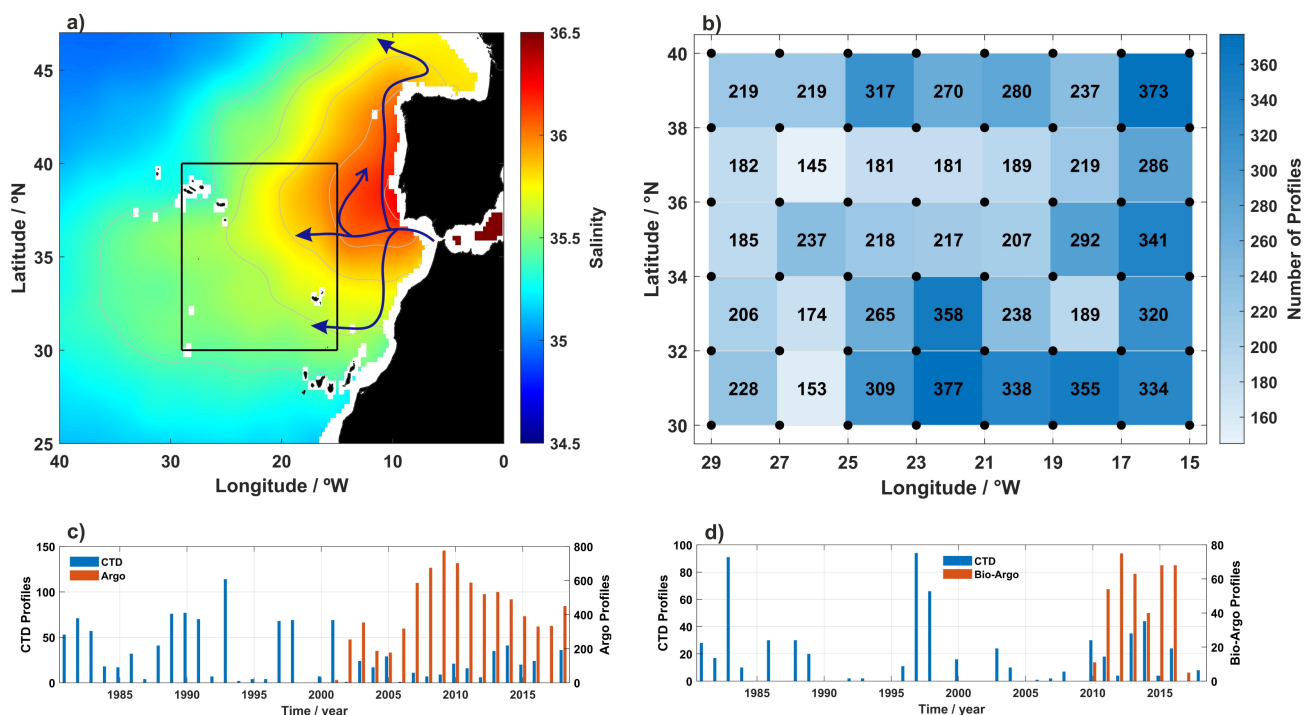


Figure 1. (a) Climatological distribution of the salinity at 1000 m from the World Ocean Atlas (WOA18) [33]. Dark blue lines are a schematic representation of the main pathways of the Mediterranean Outflow Water after exiting the Strait of Gibraltar in the eastern part of the subtropical gyre (adapted from [12,15,34]). The black box delimits the study area. (b) Number of temperature and salinity profiles for each box of the $2^\circ \times 2^\circ$ grid over the study domain in (a). Temporal distribution of temperature and salinity profiles obtained with CTD and Argo floats (c) and oxygen profiles acquired by CTD and Bio-Argo floats (d) for each year.

2. Data and Methods

2.1. Temperature, Salinity and Oxygen Time-Series

High-quality temperature, salinity, and dissolved oxygen profiles were extracted for a grid delimited by 30° N–40° N, and 29° W–15° W in the Northeast Atlantic between 1981–2018 (Figure 1a, black box). The hydrographic data were gathered from the World Ocean Database 2018 (WOD18, www.nodc.noaa.gov, accessed on 19 October 2019), PANGAEA World Data Centre (<http://www.pangaea.de>, accessed on 20 October 2019) and other data centres. For more details of the additional profiles used, see Table S1 in the Supplementary Materials. In addition, data from Argo and Bio-Argo floats was used for the period 2001–2018 and 2010–2017, respectively. The introduction of the Argo array in the early 2000s provided the first systematic and homogeneous sampling network of the ocean interior, improving both temporal and spatial resolution of ocean properties [35].

The quality assessment of the WOD18 profiles followed Wong et al. [36]. Only profiles that passed the Argo and Bio-Argo delayed-mode quality control and marked as very good data were used [37]. Additionally, salinity and temperature profiles were checked for erroneous data (i.e., density inversions, spikes and high noise profiles, systematic deviations in salinity, and missing salinity or temperature). All profiles flagged with erroneous data were removed. Dissolved oxygen data were inspected for systematic shifts relative to a mean vertical profile from the World Ocean Atlas 2018 (WOA18) [38] averaged over the region of interest in Figure 1a (black box). Since we are interested in the depths where MOW settles, profiles shallower than 1500 m were excluded. From the total of 10,592 (1716 CTD + 8876 Argo) salinity and temperature profiles and of 1222 (788 CTD + 434 Bio-Argo) dissolved oxygen profiles available in the study area, 8839 (1158 CTD + 7681 Argo, 83%) salinity and temperature profiles, and 1012 (628 CTD + 384 Bio-Argo, 83%) dissolved oxygen profiles were left (Figure 1c,d) after carrying out the described quality procedures.

Potential temperature referenced to the surface (θ , hereafter referred as temperature) and potential density (σ_θ —correspond to the surface, σ_1 —correspond to 1000 dbar) were derived for each profile [39]. In the northeast Atlantic (NEA), at intermediate levels, the MOW lies between σ_1 of 31.8 and 32.25 kg m⁻³ [10,12]. Temperature, salinity, potential density, and dissolved oxygen were interpolated at 20-dbar pressure intervals between 600–1500 dbar. The resulting profiles were then interpolated over a regular grid of 2° × 2° on a monthly basis, using the individual profiles data weighted according to the distance from the grid points (Figure 1b, black dots), assuming a 1° (≈110 km) decorrelation length scale used in the objective analysis in this study [40,41]. Integral time scales in the NEA are in the order of 30 to 40 days at 1000 m, indicating that the dominant processes at this depth are of the order of a month [42]. Therefore, the monthly averages of temperature and salinity calculated from the profiles can be assumed as statistically independent [42,43]. Thus, the annual property time-series at the core of MOW were obtained averaging the monthly mean fields over the entire study area (black box in Figure 1a) between 1000 and 1100 dbar [19,44] for both CTD and Argo datasets (Supplementary Figure S1). Anomalies were determined by subtracting the climatological mean calculated over the study area for the period 1981–2018 using all the monthly means, from the annual mean values to create anomaly property time-series of the MOW (Figure 2).

The resulting time-series were fitted using a least-square linear fit to compute the linear trends. Significant trends at 95% confidence level and confidence intervals (estimated with a t-student test) are given in bold in Table 1. The confidence intervals were calculated using the effective number of degrees of freedom [45]. The anomaly time-series were detrended to calculate the lagged correlation coefficients with the NAO. To compare the estimated trends using CTD and Argo data, we used the UK Met Office EN4 product [32] and extracted temperature and salinity for the black box of Figure 1a between 900 m and 1200 m. The EN4 resulting time-series are presented in Supplementary Figure S2.

Table 1. Estimated temperature and salinity trends and confidence intervals between 1981 and 2018, calculated for the study domain in Figure 1a. The trends were determined using only CTD data, Argo floats, combined (CTD/Argo) dataset, and EN4 dataset. Trends were calculated for each decade, and also according to NAO-phase periods. The NAO periods are divided as follows: 1981–1996 corresponds to a predominantly positive NAO; 1997–2010 comprises a period of transition from a strongly negative NAO phase (in 1996) to neutral values in the following years; and 2011–2018 corresponds to a transition of a strongly negative NAO in 2010 to a positive phase afterwards. Once the last period coincides with the last decade, the values are not repeated. Trends significant at 95% confidence level are in bold. The variance explained by the least-square linear trend (r^2) is presented in brackets. n.a. = not applicable.

	Temperature / °C year ⁻¹				Salinity / year ⁻¹			
	CTD	Argo	CTD/Argo	EN4	CTD	Argo	CTD/Argo	EN4
Decadal periods								
1981–1990	−0.022 ± 0.043 (0.13)	n.a.	−0.022 ± 0.043 (0.13)	−0.009 ± 0.012 (0.31)	−0.006 ± 0.011 (0.15)	n.a.	−0.006 ± 0.011 (0.15)	−0.001 ± 0.003 (0.08)
1991–2000	0.022 ± 0.046 (0.06)	n.a.	0.013 ± 0.036 (0.09)	−0.021 ± 0.011 (0.84)	0.009 ± 0.010 (0.29)	n.a.	0.007 ± 0.010 (0.27)	−0.005 ± 0.003 (0.79)
2001–2010	−0.017 ± 0.108 (0.03)	0.026 ± 0.049 (0.16)	0.006 ± 0.047 (0.01)	0.017 ± 0.015 (0.62)	−0.006 ± 0.019 (0.10)	0.003 ± 0.009 (0.08)	−0.001 ± 0.010 (0.01)	0.002 ± 0.002 (0.48)
2011–2018	0.050 ± 0.040 (0.71)	0.025 ± 0.013 (0.79)	0.024 ± 0.013 (0.79)	0.015 ± 0.009 (0.72)	0.007 ± 0.008 (0.49)	0.005 ± 0.003 (0.84)	0.005 ± 0.002 (0.85)	0.003 ± 0.002 (0.64)
NAO-phase periods								
1981–1996	−0.038 ± 0.021 (0.71)	n.a.	−0.038 ± 0.021 (0.71)	−0.008 ± 0.005 (0.64)	−0.009 ± 0.005 (0.70)	n.a.	−0.009 ± 0.005 (0.70)	−0.001 ± 0.001 (0.26)
1997–2010	−0.021 ± 0.053 (0.01)	0.026 ± 0.049 (0.16) ^a	−0.008 ± 0.028 (0.04)	0.013 ± 0.008 (0.67)	−0.007 ± 0.010 (0.15)	0.003 ± 0.009 (0.08) ^a	−0.003 ± 0.006 (0.02)	0.003 ± 0.002 (0.70)
Long-term mean								
1981–2018	−0.015 ± 0.007 (0.37)	0.007 ± 0.014 (0.03) ^b	−0.015 ± 0.007	−0.002 ± 0.003 (0.07)	−0.004 ± 0.002 (0.45)	−4.86 × 10 ^{−4} ± 0.003 (0.01) ^b	−0.003 ± 0.002	−2.1 × 10 ^{−4} ± 4 × 10 ^{−4} (0.01)

^a The temporal coverage of the Argo dataset starts in 2001. Thus, the trend is calculated for 2001–2010. ^b period 2001–2018.

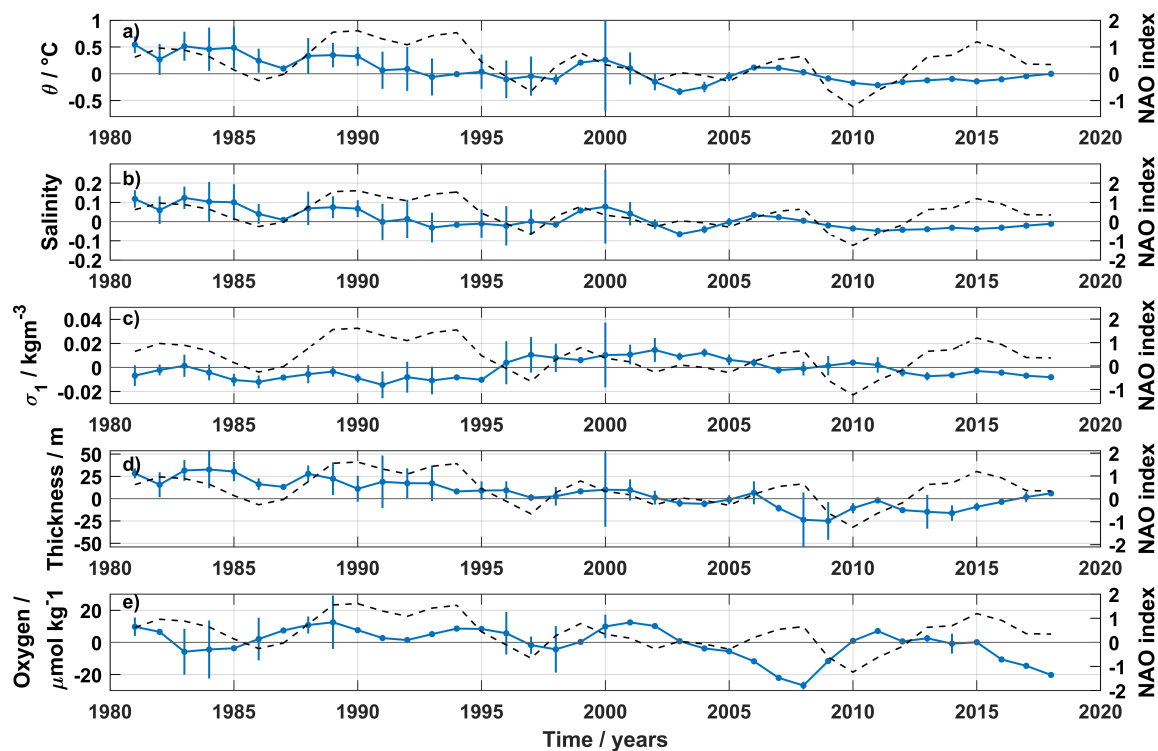


Figure 2. Annual mean anomaly time-series (1981–2018) of potential temperature (a), salinity (b), potential density (σ_1 , corresponding to 1000 dbar) (c), thickness (d) and dissolved oxygen (e) averaged at the core of MOW (between 1000 and 1100 dbar). Black dashed line is the 3-years moving mean NAO-winter index [46]. The annual anomalies were averaged over the entire study area in Figure 1a and smoothed using a 3-year moving average. Error bars represent the standard error of the mean. Points without error bars were interpolated using a 3-point mean filter.

2.2. North Atlantic Oscillation (NAO)

The North Atlantic Oscillation is the most dominant mode of interannual to decadal-scale atmospheric variability in the North Atlantic basin [47]. In this study, the winter NAO-index (December to March) was used. It is a normalized index based on the sea level pressure anomalies between Lisbon and Iceland [46].

3. Results

3.1. Interannual Variability of MOW's Properties Core

Annual mean anomaly time-series of the MOW's properties at the core are presented in Figure 2. Interannual variability (expressed as the standard deviation) is particularly striking in temperature and salinity until 2005, and in dissolved oxygen until 2010, and it is reduced afterwards (Figure 2). The variability calculated before the introduction of Argo and Bio-Argo floats might be overestimated due to the lower number of CTD profiles (Figure 1c,d), together with a sparse spatial and temporal resolution (Supplementary Figure S1).

At the MOW core, the temperature and salinity decreased over the period 1981–2018 (Figure 2a,b). However, the cooling and freshening observed were not persistent over time. Before the Argo era, the temperature and salinity decreased until 1996, followed by warming and salinification until 2000. When considering the separate datasets, after 2000, both CTD and Argo time-series differ during the first decade—the temperature and salinity time-series from CTD show a decrease until 2005, followed by a slight increase until 2010,

while the time-series using only Argo floats show the opposite behavior (Supplementary Figure S1), similar to observations presented by Soto-Navarro et al. [21] west of the Iberian Peninsula region. However, from 2010 onwards, both time-series converge to similar values with a slight increase in temperature and salinity (Supplementary Figure S1). The differences between both datasets are probably due to the different spatial and seasonal coverage of each dataset (see Supplementary Figure S1). While the Argo dataset has a more uniform temporal and spatial distribution throughout the year (Supplementary Figure S1c,d), the CTD were mostly obtained during spring and summer months (twice as many as in autumn/winter; Supplementary Figure S1b). Together with the uneven temporal resolution, the spatial distribution of the CTD profiles fails to be as homogeneous as the one provided by the Argo floats (Supplementary Figure S1a,c).

Examination of the CTD/Argo data shows, on a decadal scale, the mean temperature and salinity were highest in the 1980s (9.302 ± 0.099 °C and 35.754 ± 0.024), decreased afterwards (8.936 ± 0.144 °C and 35.677 ± 0.033 in the 1990s to 8.852 ± 0.040 °C and 35.655 ± 0.008 in the 2000s to 8.819 ± 0.019 °C and 35.641 ± 0.004 after 2011). Regarding the trends over decades, although both CTD/Argo and EN4 datasets showed a decrease in temperature and salinity during the 1980s, the trends are not significant (Table 1). In the 1990s and the 2000s, only the EN4 product shows significant trends, with freshening and cooling during the 1990s, reversing to warming and salinification after 2000. Although the combined dataset and the EN4 product disagree on the sign of the trends in the 1990s, all datasets agree with significant warming and salinification after 2010 (Table 1). The difference in trends calculated using the EN4 and the combined datasets can be attributed to various reasons. Some authors (e.g., [48,49]) attribute these differences to the data analysis methods, the way that scarce data are averaged and also to the techniques used to fill the gaps in time-series. For instance, before the Argo era, the CTD dataset's spatial coverage was too scarce and we did not interpolate the properties for all the points of the grid. Opposite to our approach, the objective analysis in the EN4 dataset combines a background climatology of the ocean state with the available profiles to calculate the temperature and salinity fields [32].

The density anomaly of the MOW core has almost no interannual variability before 1995. After 1995, the density increased over ten years, decreasing to 1980s values after 2011 (Figure 2c). Overall, the time-series shows no trends for the whole period, suggesting that the changes observed at the core are density-compensated [19].

The amount of MOW (defined here as the distance between the isopycnals $\sigma_1 = 31.8$ and $\sigma_1 = 32.25$ kg m^{-3}) decreased by -1.12 ± 0.41 m year^{-1} during the period 1981–2018. More MOW was present in the NEA until the beginning of 2000s, followed by a period of almost below-average values until 2016 (Figure 2d). In the NEA, the MOW's thickness decreases westward from the Gulf of Cadiz. We calculated a mean thickness of 470 m at 30° W and 570 m at 15° W. Our values are somewhat different from Bashmachnikov et al. [44], who calculated 400 m thickness at 30° W and ≈ 800 m at 15° W. The authors estimated the percentage of MOW in the water column, and they identified three cores of MOW, reaching deeper than 1600 m. Our estimations of MOW's thickness are restricted to the thickness between the main and the lower core of MOW [10], disregarding the mixing between the lower core of MOW and the upper North Atlantic Deep Water in the NEA. Year-to-year variability is more remarkable at the upper limit ($\sigma_1 = 31.8$ kg m^{-3}) rather than the lower limit of MOW ($\sigma_1 = 32.25$ kg m^{-3}), due to the different circulation dynamics above and below the MOW [10,12,50]. While the subtropical recirculation controls the upper limit, the lower limit is influenced by the Labrador Sea Water (LSW) circulation from the north and the Antarctic Intermediate Water (AAIW) from the south. After 2006, the upper limit's mean position deepened, reaching a more stable position after 2013. The deepening of the $\sigma_1 = 31.8$ -isopycnal might be a response to the extreme winter mixing event in 2005, leading to the formation of denser central water, that spread over the regions off the Iberian Peninsula to North Africa in the following years [51]. The lower limit was deeper until 1996, followed by 13 years with a shallower position. A thin (thicker) LSW might explain

the deepening (uplift) of the lower limit in the 1980s (1990s), allowing (restricting) the expansion of MOW into the central North Atlantic [52]. However, the authors estimated an approximate 6-years transit time of the LSW into the central Atlantic. Thus, the deepening (shallowing) of the lower limit in the 1980s (late 1990s) might be explained by thin (thicker) LSW formed during the 1970s (beginning of the 1990s). The upper limit deepened on a rate of 0.51 ± 0.37 dbar year⁻¹, while the $\sigma_1 = 32.25$ kg m⁻³ isopycnal shallowed by -0.58 ± 0.45 dbar year⁻¹ over the period 1981–2018.

The dissolved oxygen concentration decreased by -0.426 ± 0.276 $\mu\text{mol kg}^{-1}$ year⁻¹ between 1981–2018. Before 2000, the annual mean oxygen concentration at the MOW core shows low variability on an interannual scale. After 2002, the oxygen concentration decreases to a minimum in 2008. Although a weak long-term trend was estimated, the mean oxygen concentration shows more variability on a decadal-scale than on the interannual scale (Figure 2e). In a recent study, Mavropoulou et al. [53] analyzed the oxygen concentration in the Mediterranean basin, and they did not find a long-term trend since the 1960s. However, they noticed that the oxygen varied instead on an inter-decadal scale, attributing those changes to the significant deep water formation events in the eastern Mediterranean basin (known as the Eastern Mediterranean Transient in the late 1980s until mid-1990s) and in the western Mediterranean basin (the Western Mediterranean Transient between 2004–2006) [54]. In the NEA, deoxygenation at intermediate levels was also reported [55–57], and it was attributed to large scale changes in circulation as well as ventilation in connection with solubility. Additionally, a link between warming and a decrease in oxygen concentration on a global scale in the upper 1000 m layer was reported by Helm et al. [58] and Schmidtko et al. [59]. In our case, the observed weak decrease in oxygen concentration might be connected with the warming of the outflow waters in the Strait of Gibraltar [28,29].

3.2. NAO Impact at MOW Core Properties

The impact of NAO in the North Atlantic has been studied intensively in the last few decades, with reported changes in large-scale circulation, water mass properties, as well as on the ecosystems level. Although the effect of NAO affects the upper water column primarily, some authors observed the influence of NAO in water mass changes and properties at intermediate depths [28,30,52].

The temperature and salinity anomaly time-series at the core show a correlation with the NAO, with correlation coefficients of 0.38 and 0.29 (both with $p < 0.05$), respectively (Figures 2a,b and 3a). However, the effect of NAO at such depths is not immediate, and it is “felt” with delay. The strongest correlation between temperature and salinity anomalies with NAO occur with a lag of 8 (0.51, $p < 0.05$) and 7 years (0.45, $p < 0.05$), respectively, with both properties lagging the NAO (Figure 3a).

The cross-correlation between the anomaly time-series from the EN4 gridded product and NAO are presented in Figure 3b. Although there are differences between these time-series and the combined CTD/Argo dataset (see Supplementary Figure S3), the maximum correlation coefficients are observed for the same time-lag in temperature (7 years, $\rho = 0.57$, $p < 0.05$) and salinity (8 years, $\rho = 0.44$, $p < 0.05$). Time-scales of the same order were interpreted by Eden & Willebrand [60] as a delayed baroclinic ocean response to the NAO. The density anomaly at the core and the NAO are strongly correlated at 0 lag (-0.50 , $p < 0.05$) and at 7 years (-0.41 , $p < 0.05$), supporting the delayed response of the ocean to NAO.

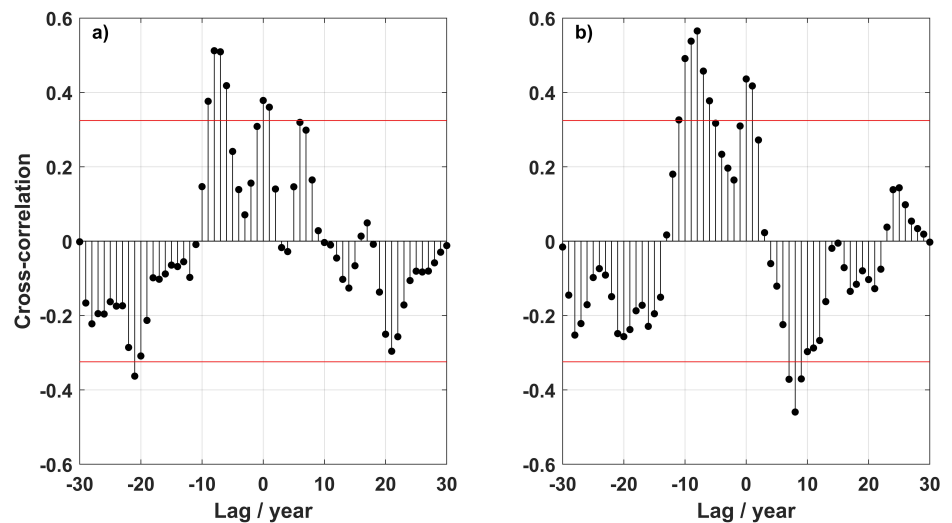


Figure 3. (a) Cross-correlation between the North Atlantic Oscillation and the CTD/Argo temperature detrended anomaly time-series, and the EN4 temperature anomaly time-series (b). The cross-correlation was calculated using 3-years running mean of both NAO-winter index and the annual mean temperature anomaly time-series. Red lines represent the upper and lower 95% confidence bounds.

4. Discussion

We have shown that the changes in the MOW's properties at the core (temperature, salinity and dissolved oxygen) and also the MOW's thickness changed in the last 40 years, at inter-annual to decadal time-scales.

The outflow of the Mediterranean Water through the Strait of Gibraltar is mainly composed of a mixture of intermediate and deep waters—the Levantine Intermediate Water (LIW) and the Western Mediterranean Deep Water (WMDW). The LIW is formed through open-sea convection in the eastern Mediterranean basin and flows across the Strait of Sicily into the western basin [61]. The WMDW is formed in the Gulf of Lion by winter deep convection [62] and flows through the Strait of Gibraltar. Recently, Millot et al. [24] showed that the Tyrrhenian Deep Water (TDW) contributed to the outflow water composition after the 2000s.

Since 1981, we estimated cooling of $-0.015 \pm 0.007 \text{ }^\circ\text{C year}^{-1}$ and freshening by $-0.003 \pm 0.002 \text{ year}^{-1}$ at the core of MOW in the northeast Atlantic using the CTD/Argo dataset (Table 1). Over the recent years, most trends estimated for the MOW's properties in the North Atlantic were calculated for time-series shorter than 20 years, with just a few studies using time-series longer than 40 years (Table 2). Until the early 1980s, the trends calculated in the NEA showed clear warming and salinification at intermediate depths (Table 2), following the warming and salinification of the Mediterranean waters. However, after the 1980s, some authors reported cooling and freshening (e.g., [20,23]), or no trends at all (Table 1 in [21]) in the NEA, while the waters in the Mediterranean basin continued to warm and get saltier.

The calculated trends in the NEA after the 1980s contradict the warming and salinification of the intermediate and deep waters in the Mediterranean basin reported since the 1950s, as well as for the outflow waters into the North Atlantic (Table 2). One reason might be the dilution of the outflow waters at the Strait of Gibraltar. In the NEA, the highest percentage of around 50–60% of MOW is found at the main core layer of MOW (900 m–1000 m) [44]. However, the percentage of MOW at the core decreases substantially westward, reaching values below 40% for the lower core south of the Azores region [44]. Also, Fiúza et al. [63] estimated that the lower core dilutes 0.06/100 km in salinity and 0.05 $^\circ\text{C}/100 \text{ km}$ in temperature for the northward pathways along the western Iberian Peninsula. A careful inspection of the trends calculated for the Mediterranean basin and

also for the outflow waters reveals that those trends are of the order of 10^{-3} for periods longer than 20 years (Table 2). Considering that after MOW leaves the Strait of Gibraltar, the outflow waters experience strong mixing in the Gulf of Cadiz region, it is possible that the trends calculated for the NEA over such long periods might be not significant or even reversed. Leadbetter et al. [20] suggested that the warming observed between 1981 and 2005 was due to change in the source water, as also reported by Millot et al. [24]. However, Lozier & Sindlinger [25] using a box model showed that source water changes have almost no impact on interannual to decadal variability of MOW's properties. In the same study, the authors suggested that changes in the North Atlantic basin circulation alter the main pathways of MOW, and in consequence, the properties of MOW.

To investigate whether the different NAO phases would possibly influence the detection of different MOW core properties, we divided the properties time-series into different periods. Between 1981 and 1996, the NAO was predominantly in a positive phase. During this period, the MOW core cooled and freshened (Table 1). After the negative NAO in 1997, the NAO index was rather neutral until 2010, and the MOW's properties at the core do not show any significant trend for the combined dataset (Table 1). Using the EN4 dataset, the MOW core during this period was warmer and saltier. In contrast, after the NAO negative phase in 2010, the NAO return to a more positive phase, and the MOW core warmed and became saltier (Table 1).

The reverse of trends at the MOW core in the NEA seems to be an indirect response to the NAO-phase, in a way that a positive (negative) NAO phases induce a more westward (northward) MOW propagation. Thus, the trends detected in our study area might be related to the expansion/retraction of the MOW tongue. The mean salinity distribution around the MOW core during a period of predominantly negative NAO (1965–1974) and positive NAO (1985–1994) are presented in Figure 4a,b, together with the salinity difference between the two periods (Figure 4c). Since the changes at the MOW core in the NEA are density-compensated, only the salinity is shown. During a negative NAO-phase, the expansion of the MOW tongue westward is more restricted compared with the positive NAO-phase (Figure 4a,b, red colours). In contrast, the salinity is higher along the northward pathway of MOW during a negative NAO-phase. The difference between the two periods enables a better view of the dynamic of MOW in the NEA. A negative anomaly of salinity appears along the westward pathway of MOW in contrast with a positive anomaly along the northward MOW pathway (Figure 4c). The northward penetration of MOW was already studied by several authors (e.g., [25,31,64]). These authors showed that during periods of negative (positive) NAO-phase, the Subpolar Front shifts westward (eastward), allowing (blocking) the penetration of the MOW into higher latitude, into the Subpolar gyre. Also, Chaudhuri et al. [27] and Bozec et al. [26], using model simulations, showed that under different NAO-phases, the circulation and distribution of water masses at intermediate depths in the North Atlantic is different. At times of a positive NAO-phase, the flow of MOW into higher latitudes is blocked, and a westward extension of the MOW tongue is observed [26,27] (Figure 4b). The warming and salinification of MOW reported by Potter & Lozier [19] and Leadbetter et al. [20] covered a long period of negative NAO in the 1950s and 1960s shifting to a positive phase in the late 1970s [65]. In contrary, the cooling and freshening calculated by Leadbetter et al. [20] at 36° N after 1981 comprise a time-span of positive and neutral values of NAO (after a strongly negative NAO in 1996). Also, during the neutral phase of NAO in the 2000s, no trends were determined in the NEA (Table 1 in [21]).

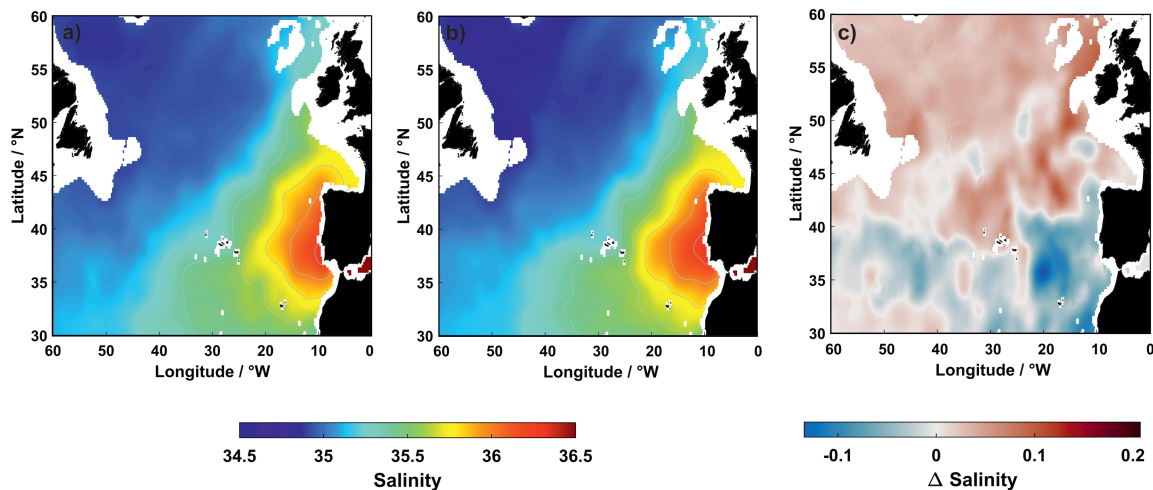


Figure 4. (a) Salinity distribution averaged at the core of Mediterranean Outflow Water (MOW) (1000–1100 m) from the World Ocean Atlas (WOA18 in [33]) between 1965–1974 and (b) between 1985–1994. (c) Salinity difference between the periods 1965–1974 and 1985–1994.

Table 2. Summary of in situ potential temperature and salinity trends in the Northeast Atlantic basin, at the Strait of Gibraltar and in the Mediterranean Sea. The period refers to the considered time span for which the trends were calculated. The dataset gives the source used. n.s.: trends are not significant; n.a. not applicable in the considered study.

Area	Period	Dataset	Depth Range (m)	Trend		Reference
				Temperature	Salinity	
North Atlantic basin						
30°–40° N; 20°–5° W	1955–1993	CTD	1150	0.101 °C/decade	0.0283/decade	[19]
32°–42° N; 25°–10° W	1955–2003	HYDROBASE2	1100	0.119 °C/decade	0.024/decade	[26]
28°–42° N; 24°–5° W	2002–2010	Argo	600–1200	n.s.	n.s.	[21]
Kiel 276 (33° N, 22° W)	1980–2009	Mooring	1000	0.03 °C/y ^a	n.a.	[42]
Bay of Biscay/43°30′–43°54′ N; 3°47′ W	1995–2003	CTD	700–1000	0.023 °C/y	0.005/y	[22]
Bay of Biscay/43.5–48° N; 10°–1° W	2004–2013	Argo	600–1200	−0.011 °C/y	−0.005/y	[23]
24.5° N; 35°–25° W	1957–2004	CTD	900–1750	0.0014 °C/y	−0.0002/y	[66]
53° N; 25°–15° W	1992–2002	CTD	27.45 < σ_θ < 27.65	0.049 °C/y	0.0088/y	[64]
32°S–36° N	1920–1990	CTD	1000–2000	0.005 °C/y	n.d.	[18]
Gulf of Cadiz/35.5°–37° N; 9°–5.9° W	1948–1999	MEDATALAS II + WOD2005	700–1400	0.16°/decade	0.05/decade	[67]
Strait of Gibraltar						
Espartel sill/35°51.70′ N; 5°58.60′ W	2004–2010	Mooring	≈360	0.0017 °C/y	−0.0022/y	[21]
	2005–2009	Mooring	≈360	0.0091 °C/y	−0.0056/y	[68]
	2005–2016	Mooring	≈360	0.0069 °C/y	0.0013/y	[29]
Eastern Strait	2009–2014	CTD	WMDW	0.009 °C/y	0.003/y	[69]
Mediterranean basin						
Western Mediterranean	1943–2000	Medatlas 2002	600–bottom	0.002 °C/y	9.2 × 10 ^{−4} /y	[70]
Western Mediterranean	1943–2015	Medatlas + RADMED	600–bottom	0.004 °C/y	0.001/y	[71]
MEDOC area	1969–1987	CTD	1850–2050	0.0027 °C/y	0.0019/y	[72]
Balearic Sea	1996–2005	CTD	600–bottom	0.011 °C/y	0.003/y	[73]
Africa-42° N; 0°–10° E	1909–1955	NODC + CTD	2000	8.19 × 10 ^{−4} °C/y	3.88 × 10 ^{−4}	[74]
	1955–1989	NODC + CTD	2000	0.0016 °C/y	9.45 × 10 ^{−4}	[74]
Western basin	1959–1994	CTD	2000–bottom	0.0036 °C/y ^a	0.0011/y	[75]
38°–46° N; 0°–10° E	1955–2006	CTD + Argo	WMDW	0.0036 °C/y	0.0015/y	[76]
DYFAMED site/WMDW	1995–2004	MEDATLAS II	400–1200	0.012 °C/y	0.0043/y	[77]
DYFAMED site	1995–2004	CTD	1800	0.0054 °C/y	0.002/y	[78]
DYFAMED site	1995–2005	CTD	1974	0.005 °C/y	0.0022/y	[79]
Gulf of Lion	1960–1994	CTD	1000–bottom	0.0016 °C/y	8 × 10 ^{−4} /y	[28]
Gulf of Lion	2009–2013	Mooring + Buoy + CTD	1000–2300	0.0032 °C/y	0.0033/y	[80]
Tyrrhenian sea	1996–2001	Mooring	>3000	0.016 °C/y	0.008/y	[81]
Ligurian Sea	1950–1973	CTD	300–400	0.0068 °C/y	0.0018/y	[75]
Western basin/LIW	1943–2000	CTD	500	0.004 °C/y	0.0011/y	[82]
Western basin/LIW	1943–2000	CTD	200–600	0.0005 °C/y	13 × 10 ^{−4} /y	[70]
41°–42° N; 5°–7.5° E	1990–2005	CTD + Argo	500–600	n.s.	9.17 × 10 ^{−4}	[76]
Levantine Basin/LIW	1979–2014	CTD	≈150–350	0.03 °C/y	0.005/y	[83]

^a Trend was calculated using in situ temperature.

5. Conclusions

In the Northeast Atlantic, the MOW experience periods of cooling/freshening and warming/salinification from 1981 onwards, after a prolonged period of warming and salinification since the 1950s. The temperature and salinity increased in the last decade (2011 onwards), after a long period of cooling and freshening (1981–1996). The opposite trends at the MOW core seems to be related to the different phases of NAO. During a prolonged positive NAO-phase (1981–1996), the temperature and salinity decreased. In contrast, warming and salinification were observed after the NAO-phase changed from negative to positive (from 2011 onwards). The different direction of trends detected in the NEA can be interpreted as an adjustment of the large scale circulation at intermediate depths in response to the NAO-phase, insofar a positive NAO-phase induce a more westward MOW propagation in opposition to a negative NAO-phase, where the MOW propagation is preferentially northward. However, the NAO-phase effect at intermediate depths leads the changes at the core properties by 7–8 years. The oxygen concentration at the core also decreased after 1981, but no connection to the NAO was found. The oxygen concentration at the MOW shows more inter-decadal variability, most likely linked to the variability on decadal-scale, associated with the different deep water formation events in the Mediterranean Sea. Also, the decrease in oxygen concentration might be connected to the warming of the outflow waters, which decreases the solubility of oxygen. However, we should point out that the effect of biological activity on dissolved oxygen levels was not considered.

The results presented here indicate weak cooling and freshening over the entire period in both datasets (CTD/Argo and EN4 product) for the region studied. It is important to note that the trends calculated are averaged for the entire box in Figure 1a, and might not translate all the dynamics in the study area or in a different (sub)domain. Although the results for the individual periods or decades are partly contradicting each other, they highlight the importance of a careful choice of the dataset for analyzing climate signals at mid-depths.

Supplementary Materials: The following are available online at <https://www.mdpi.com/2673-1924/2/1/16/s1>, Figure S1. (a) Number of temperature and salinity CTD profiles for each box of the $2^\circ \times 2^\circ$ grid over the study domain in Figure 1a. (b) Histogram with the number of CTD profiles per season. (c) Same as (a) but for the number of Argo floats. (d) Same as (b) but with respect to the number of Argo floats. Figure S2. Annual mean potential temperature (a), salinity (b), potential density (with reference to 1000 dbar) (c), thickness (d), and dissolved oxygen concentration (e) averaged at the core of MOW (between 1000 and 1100 dbar). The blue time-series were calculated using only CTD profiles, and the red time-series were determined using only Argo/Bio-Argo profiles. Black dashed time-series are the 3-years moving mean winter NAO-index. The annual means were averaged over the entire domain of Figure 1a and smoothed with a 3-years running mean. Error bars represent the standard error of the mean. Points without error bars were interpolated using a 3-point moving mean filter. Figure S3. Annual mean potential temperature (a), and salinity (b) averaged at the core of MOW (between 1000 and 1100 dbar). The blue time-series were calculated using the combined CTD and Argo profiles, and the yellow time-series were determined using the EN4 gridded product. The annual means were averaged over the entire domain of Figure 1a and smoothed with a 3-years running mean. Error bars represent the standard error of the mean. Points without error bars were interpolated using a 3-point moving mean filter. Table S1. Hydrographic data used from cruises in the Northeast Atlantic within the study domain of Figure 1a obtained from the PANGAEA, ICES repository, CCHDO, and BODC data centres for the period 1981–2018. The date format includes the month and year.

Author Contributions: Conceptualization H.C.F.; data analysis H.C.F.; writing—original draft preparation, H.C.F.; writing—review and editing, H.C.F., J.J.W.; funding acquisition, J.J.W. All authors have read and agreed to the published version of the manuscript.

Funding: J.J.W. thanks the Deutsche Forschungsgemeinschaft (DFG) for many years of financial support for cruises in the study area during various projects (WA2175/1-1 to 2175/5-1).

Data Availability Statement: Argo data were collected and made freely available by the International Argo Programme and the national programmes that contribute to it. The Argo Programme is part of the Global Ocean Observation System. Objective analysis fields were obtained from the UK Met Office EN4 product (<http://www.metoffice.gov.uk/hadobs/en4/>, accessed on 18 October 2020).

Acknowledgments: We thank the many investigators who contribute to the databases and all people on board of numerous cruises used in this study. We also thank the three anonymous reviewers for valuable suggestions to improve our study.

Conflicts of Interest: The authors declare no conflict of interest. The funders had no role in the design of the study; in the collection, analyses, or interpretation of data; in the writing of the manuscript, or in the decision to publish the results.

Abbreviations

The following abbreviations are used in this manuscript:

AAIW	Antarctic Intermediate Water
CTD	Conductivity, Temperature, Depth
LIW	Levantine Intermediate Water
LSW	Labrador Sea Water
MOW	Mediterranean Outflow Water
NAO	North Atlantic Oscillation
NEA	Northeast Atlantic
TDW	Tyrrhenian Deep Water
WMDW	Western Mediterranean Deep Water
WOA	World Ocean Atlas
WOD	World Ocean Database

References

- Zenk, W. On the Mediterranean outflow west of Gibraltar. *Meteor-Forschungsergebnisse A* **1975**, *16*, 35–43.
- Ambar, I.; Howe, M.R.; Abdullah, M.I. A Physical and Chemical Description of the Mediterranean Outflow in the Gulf of Cadiz. *Dtsch. Hydrogr. Z.* **1976**, *29*, 58–68. [[CrossRef](#)]
- Reid, J.L. On the contribution of the Mediterranean Sea outflow to the Norwegian-Greenland Sea. *Deep-Sea Res. Part A Oceanogr. Res. Pap.* **1979**, *26*, 1199–1223. [[CrossRef](#)]
- Bower, A.S.; Serra, N.; Ambar, I. Structure of the Mediterranean Undercurrent and Mediterranean Water spreading around the southwestern Iberian Peninsula. *J. Geophys. Res.* **2002**, *107*, 3161. [[CrossRef](#)]
- Reid, J.L. On the Middepth Circulation and Salinity Field in the North Atlantic Ocean. *J. Geophys. Res.* **1978**, *83*, 5063–5067. [[CrossRef](#)]
- Iorga, M.C.; Lozier, M.S. Signatures of the Mediterranean outflow from a North Atlantic climatology: 1. Salinity and density fields. *J. Geophys. Res.* **1999**, *104*, 25985–26009. [[CrossRef](#)]
- Serra, N.; Ambar, I.; Käse, R.H. Observations and numerical modelling of the Mediterranean outflow splitting and eddy generation. *Deep-Sea Res. II* **2005**, *52*, 383–408. [[CrossRef](#)]
- Armi, L.; Zenk, W. Large Lenses of Highly Saline Mediterranean Water. *J. Phys. Oceanogr.* **1984**, *14*, 1560–1576. [[CrossRef](#)]
- Richardson, P.L.; McCartney, M.S.; Maillard, C. A search for meddies in historical data. *Dyn. Atmos. Ocean.* **1991**, *15*, 241–265. [[CrossRef](#)]
- van Aken, H.M. The hydrography of the mid-latitude Northeast Atlantic Ocean II: The intermediate water masses. *Deep-Sea Res. I* **2000**, *47*, 789–824. [[CrossRef](#)]
- Siedler, G.; Armi, L.; Müller, T.J. Meddies and decadal changes at the Azores Front from 1980 to 2000. *Deep-Sea Res. II* **2005**, *52*, 583–604. [[CrossRef](#)]
- Carracedo, L.I.; Gilcoto, M.; Mercier, H.; Pérez, F.F. Seasonal dynamics in the Azores-Gibraltar Strait region: A climatologically-based study. *Prog. Oceanogr.* **2014**, *122*, 116–130. [[CrossRef](#)]
- Sánchez-Leal, R.F.; Bellanco, M.J.; Fernández-Salas, L.M.; García-Lafuente, J.; Gasser-Rubinat, M.; González-Pola, C.; Hernández-Molina, F.J.; Pelegrí, J.L.; Peliz, A.; Relvas, P.; et al. The Mediterranean Overflow in the Gulf of Cadiz: A rugged journey. *Sci. Adv.* **2017**, *3*, eaao0609. [[CrossRef](#)] [[PubMed](#)]
- Izquierdo, A.; Mikolajewicz, U. The role of tides in the spreading of Mediterranean Outflow waters along the southwestern Iberian margin. *Ocean. Model.* **2019**, *133*, 27–43. [[CrossRef](#)]
- de Pascual-Collar, Á.; Sotillo, M.G.; Levier, B.; Aznar, R.; Lorente, P.; Amo-Baladrón, A.; Álvarez-Fanjul, E. Regional circulation patterns of Mediterranean Outflow Water near the Iberian and African continental slopes. *Ocean Sci.* **2019**, *15*, 565–582. [[CrossRef](#)]

16. Candela, J. Chapter 5.7 Mediterranean water and global circulation. In *Ocean Circulation and Climate*; Siedler, G., Church, J., Gould, J., Eds.; Academic Press: Cambridge, MA, USA, 2001; Volume 77, pp. 417–429. [[CrossRef](#)]
17. Levitus, S.; Antonov, J.I.; Boyer, T.P.; Stephens, C. Warming of the World Ocean. *Science* **2000**, *287*, 2225–2229. [[CrossRef](#)]
18. Arbic, B.K.; Owens, W.B. Climatic Warming of Atlantic Intermediate Waters. *J. Clim.* **2001**, *14*, 4091–4108. [[CrossRef](#)]
19. Potter, R.A.; Lozier, M.S. On the warming and salinification of the Mediterranean outflow waters in the North Atlantic. *Geophys. Res. Lett.* **2004**, *31*, L01202. [[CrossRef](#)]
20. Leadbetter, S.J.; Williams, R.G.; McDonagh, E.L.; King, B.A. A twenty year reversal in water mass trends in the subtropical North Atlantic. *Geophys. Res. Lett.* **2007**, *34*, L12608. [[CrossRef](#)]
21. Soto-Navarro, J.; Criado-Aldeanueva, F.; Sánchez-Garrido, J.C.; García-Lafuente, J. Recent thermohaline trends of the Atlantic waters inflowing to the Mediterranean Sea. *Geophys. Res. Lett.* **2012**, *39*, L01604. [[CrossRef](#)]
22. González-Pola, C.; Lavín, A.; Vargas-Yáñez, M. Intense warming and salinity modification of intermediate water masses in the southeastern corner of the Bay of Biscay for the period 1992–2003. *J. Geophys. Res.* **2005**, *110*, C05020. [[CrossRef](#)]
23. Costoya, X.; deCastro, M.; Gómez-Gesteira, M. Thermocline trends in the Bay of Biscay from Argo floats over the decade 2004–2013. *J. Mar. Syst.* **2014**, *139*, 159–165. [[CrossRef](#)]
24. Millot, C.; Candela, J.; Fuda, J.L.; Tber, Y. Large warming and salinification of the Mediterranean outflow due to changes in its composition. *Deep-Sea Res. I* **2006**, *53*, 656–666. [[CrossRef](#)]
25. Lozier, M.S.; Sindlinger, L. On the Source of Mediterranean Overflow Water Property Changes. *J. Phys. Oceanogr.* **2009**, *39*, 1800–1817. [[CrossRef](#)]
26. Bozec, A.; Lozier, M.S.; Chassignet, E.P.; Halliwell, G.R. On the variability of the Mediterranean Outflow Water in the North Atlantic from 1948 to 2006. *J. Geophys. Res.* **2011**, *116*, C09033. [[CrossRef](#)]
27. Chaudhuri, A.H.; Gangopadhyay, A.; Bisagni, J.J. Contrasting Response of the Eastern and Western North Atlantic Circulation to an Episodic Climate Event. *J. Phys. Oceanogr.* **2011**, *41*, 1630–1638. [[CrossRef](#)]
28. Krahnemann, G.; Schott, F. Longterm increases in Western Mediterranean salinities and temperatures: Anthropogenic and climatic sources. *Geophys. Res. Lett.* **1998**, *25*, 4209–4212. [[CrossRef](#)]
29. Naranjo, C.; García-Lafuente, J.; Sammartino, S.; Sánchez-Garrido, J.C.; Sánchez-Leal, R.; Jesús Bellanco, M. Recent changes (2004–2016) of temperature and salinity in the Mediterranean outflow. *Geophys. Res. Lett.* **2017**, *44*, 5665–5672. [[CrossRef](#)]
30. Dickson, R.; Lazier, J.; Meincke, J.; Rhines, P.; Swift, J. Long-term coordinated changes in the convective activity of the North Atlantic. *Prog. Oceanogr.* **1996**, *38*, 241–295. [[CrossRef](#)]
31. Lozier, M.S.; Steward, N.M. On the Temporally Varying Northward Penetration of Mediterranean Overflow Water and Eastward Penetration of Labrador Sea Water. *J. Phys. Oceanogr.* **2008**, *38*, 2097–2103. [[CrossRef](#)]
32. Good, S.A.; Martin, M.J.; Rayner, N.A. EN4: Quality controlled ocean temperature and salinity profiles and monthly objective analyses with uncertainty estimates. *J. Geophys. Res. Ocean.* **2013**, *118*, 6704–6716. [[CrossRef](#)]
33. Zweng, M.M.; Reagan, J.R.; Seidov, D.; Boyer, T.P.; Locarnini, R.A.; Garcia, H.E.; Mishonov, A.V.; Baranova, O.K.; Weathers, K.; Paver, C.R.; et al. *World Ocean Atlas 2018, Volume 2: Salinity*; NOAA Atlas NESDIS 82; NOAA: Washington, DC, USA, 2018; p. 50.
34. Danialt, N.; Mercier, H.; Lherminier, P.; Sarafanov, A.; Falina, A.; Zunino, P.; Pérez, F.F.; Ríos, A.F.; Ferron, B.; Huck, T.; et al. The northern North Atlantic Ocean mean circulation in the early 21st century. *Prog. Oceanogr.* **2016**, *146*, 142–158. [[CrossRef](#)]
35. Wong, A.; Wijffels, S.E.; Riser, S.C.; Pouliquen, S.; Hosoda, S.; Roemmich, D.; Gilson, J.; Johnson, G.C.; Martini, K.; Murphy, D.J.; et al. Argo Data 1999–2019: Two Million Temperature-Salinity Profiles and Subsurface Velocity Observations From a Global Array of Profiling Floats. *Front. Mar. Sci.* **2020**, *7*, 700. [[CrossRef](#)]
36. Wong, A.; Keeley, R.; Carval, T.; Argo Data Management Team. *Argo Quality Control Manual for CTD and Trajectory Data*; Ifremer: Brest, France, January 2020. [[CrossRef](#)]
37. Argo. Argo float data and metadata from Global Data Assembly Centre (Argo GDAC). *SEANOE* **2000**. [[CrossRef](#)]
38. Garcia, H.E.; Weather, K.; Paver, C.R.; Smolyar, I.; Boyer, T.P.; Locarnini, R.A.; Zweng, M.M.; Mishonov, A.V.; Baranova, O.K.; Seidov, D.; et al. *World Ocean Atlas 2018, Volume 3: Dissolved Oxygen, Apparent Oxygen Utilization, and Oxygen Saturation*; A. Mishonov Technical Editor; NOAA Atlas NESDIS 83; NOAA: Washington, DC, USA, 2018; p. 38.
39. UNESCO. Algorithms for Computation of Fundamental Properties of Seawater. *UNESCO Tech. Pap. Mar. Sci.* **1983**, *44*, 1–53.
40. Barnes, S.L. *Mesoscale Objective Map Analysis Using Weighted Time-Series Observations*; NOAA Technical Memorandum ERL NSSL 62; NOAA: Washington, DC, USA, 1973.
41. Pierce, S. Stephen Pierce (2020). Barnes Objective Analysis. 2010. Available online: <https://www.mathworks.com/matlabcentral/fileexchange/28666-barnes-objective-analysis> (accessed on 15 November 2020).
42. Frazão, H.C.; Prien, R.D.; Müller, T.J.; Schulz-Bull, D.E.; Waniek, J.J. 30 years of temporal variability of temperature and currents below the main thermocline between 1980–2009 in the subtropical Northeast Atlantic (Kiel 276, 33°N, 22°W). *J. Mar. Syst.* **2021**, *217*, 103517. [[CrossRef](#)]
43. Müller, T.J.; Waniek, J.J. *KIEL276 Time Series Data from Moored Current Meters 33°N, 22°W, 5285 m Water Depth. March 1980–April 2011. Background Information and Data Compilation*; GEOMAR Report Nr. 13; GEOMAR: Kiel, Germany, 2013. [[CrossRef](#)]
44. Bashmachnikov, I.; Nascimento, A.; Neves, F.; Menezes, T.; Koldunov, N.V. Distribution of intermediate water masses in the subtropical northeast Atlantic. *Ocean. Sci.* **2015**, *11*, 803–827. [[CrossRef](#)]
45. Thomson, R.E.; Emery, W.J. Chapter 3—Statistical Methods and Error Handling. In *Data Analysis Methods in Physical Oceanography*, 3rd ed.; Thomson, R.E., Emery, W.J., Eds.; Elsevier: Amsterdam, The Netherlands, 2014; pp. 219–311. [[CrossRef](#)]

46. Hurrell, J. The Climate Data Guide: Hurrell North Atlantic Oscillation (NAO) Index (Station-Based). 2020. Available online: <https://climatedataguide.ucar.edu/climate-data/hurrell-north-atlantic-oscillation-nao-index-station-based> (accessed on 4 March 2020).
47. Hurrell, J.; Kushnir, Y.; Ottersen, G.; Visbeck, M. An overview of the North Atlantic oscillation. *Geophys. Monogr. Am. Geophys. Union* **2003**, *134*, 1–36.
48. Hurrell, J.W.; Trenberth, K.E. Global Sea Surface Temperature Analyses: Multiple Problems and Their Implications for Climate Analysis, Modeling, and Reanalysis. *Bull. Am. Meteorol. Soc.* **1999**, *80*, 2661–2678. [[CrossRef](#)]
49. Gregory, J.M.; Banks, H.T.; Stott, P.A.; Lowe, J.A.; Palmer, M.D. Simulated and observed decadal variability in ocean heat content. *Geophys. Res. Lett.* **2004**, *31*, L15312. [[CrossRef](#)]
50. Käse, R.; Zenk, W. Structure of the Mediterranean Water and meddy characteristics in the northeastern Atlantic. In *The Warmwatersphere of the North Atlantic Ocean*; Krauss, W., Ed.; Gebrüder Borntraeger: Berlin, Germany, 1996; pp. 365–395.
51. Somavilla, R.; González-Pola, C.; Rodríguez, C.; Josey, S.A.; Sánchez, R.F.; Lavín, A. Large changes in the hydrographic structure of the Bay of Biscay after the extreme mixing of winter 2005. *J. Geophys. Res.* **2009**, *114*, C01001. [[CrossRef](#)]
52. Curry, R.G.; McCartney, M.S.; Joyce, T.M. Oceanic transport of subpolar climate signals to mid-depth subtropical waters. *Nature* **1998**, *391*, 575–577. [[CrossRef](#)]
53. Mavropoulou, A.M.; Vervatis, V.; Sofianos, S. Dissolved oxygen variability in the Mediterranean Sea. *J. Mar. Syst.* **2020**, *208*, 103348. [[CrossRef](#)]
54. Schroeder, K.; Chiggiato, J.; Bryden, H.L.; Borghini, M.; Ismail, S.B. Abrupt climate shift in the Western Mediterranean Sea. *Sci. Rep.* **2016**, *6*, 23009. [[CrossRef](#)]
55. Johnson, G.C.; Gruber, N. Decadal water mass variations along 20°W in the Northeastern Atlantic Ocean. *Prog. Oceanogr.* **2007**, *73*, 277–295. [[CrossRef](#)]
56. Stendero, I.; Gruber, N. Oxygen trends over five decades in the North Atlantic. *J. Geophys. Res.* **2012**, *117*, C11004. [[CrossRef](#)]
57. Stendero, I.; Kieke, D.; Rhein, M.; Gruber, N.; Steinfeldt, R. Interannual to decadal oxygen variability in the mid-depth water masses of the eastern North Atlantic. *Deep-Sea Res. I* **2015**, *95*, 85–98. [[CrossRef](#)]
58. Helm, K.P.; Bindoff, N.L.; Church, J.A. Observed decreases in oxygen content of the global ocean. *Geophys. Res. Lett.* **2011**, *38*, L23602. [[CrossRef](#)]
59. Schmidtko, S.; Stramma, L.; Visbeck, M. Decline in global oceanic oxygen content during the past five decades. *Nature* **2017**, *542*, 335–339. [[CrossRef](#)]
60. Eden, C.; Willebrand, J. Mechanism of Interannual to Decadal Variability of the North Atlantic Circulation. *J. Clim.* **2001**, *14*, 2266–2280. [[CrossRef](#)]
61. Katz, E.J. The Levantine Intermediate Water between the Strait of Sicily and the Strait of Gibraltar. *Deep-Sea Res.* **1972**, *19*, 507–520. [[CrossRef](#)]
62. Stommel, H. Deep winter-time convection in the Western Mediterranean Sea. In *Studies in Physical Oceanography*; Gordon, A.L., Ed.; Gordon and Breach: New York, NY, USA, 1972; Volume 2, pp. 207–218.
63. Fiúza, A.F.G.; Hamann, M.; Ambar, I.; Díaz del Río, G.; González, N.; Cabanas, J.M. Water masses and their circulation off western Iberian during May 1993. *Deep-Sea Res. I* **1998**, *45*, 1127–1160. [[CrossRef](#)]
64. Sarafanov, A.; Falina, A.; Sokov, A.; Demidov, A. Intense warming and salinification of intermediate waters of southern origin in the eastern subpolar North Atlantic in the 1990s to mid-2000s. *J. Geophys. Res.* **2008**, *113*, C12022. [[CrossRef](#)]
65. Hurrell, J. Decadal trends in the North Atlantic Oscillation: Regional temperatures and precipitation. *Science* **1995**, *269*, 676–679. [[CrossRef](#)] [[PubMed](#)]
66. Cunningham, S.A.; Alderson, S. Transatlantic temperature and salinity changes at 24.5°N from 1957 to 2004. *Geophys. Res. Lett.* **2007**, *34*, L14606. [[CrossRef](#)]
67. Fusco, G.; Artale, V.; Cotroneo, Y.; Sannino, G. Thermohaline variability of Mediterranean Water in the Gulf of Cadiz, 1948–1999. *Deep-Sea Res. I* **2008**, *55*, 1624–1638. [[CrossRef](#)]
68. García-Lafuente, J.; Delgado, J.; Sánchez Román, A.; Soto, J.; Carracedo, L.; Díaz del Río, G. Interannual variability of the Mediterranean outflow observed in Espartel sill, western Strait of Gibraltar. *J. Geophys. Res. Ocean.* **2009**, *114*, C10018. [[CrossRef](#)]
69. Naranjo, C.; Sammartino, S.; García-Lafuente, J.; Bellanco, M.J.; Taupier-Letage, I. Mediterranean waters along and across the Strait of Gibraltar, characterization and zonal modification. *Deep. Sea Res. Part I* **2015**, *105*, 41–52. [[CrossRef](#)]
70. Vargas-Yáñez, M.; Zunino, P.; Benali, A.; Delpy, M.; Pastre, F.; Moya, F.; García-Martínez, M.D.C.; Tel, E. How much is the western Mediterranean really warming and salting? *J. Geophys. Res. Ocean.* **2010**, *115*, C04001. [[CrossRef](#)]
71. Vargas-Yáñez, M.; García-Martínez, M.C.; Moya, F.; Balbín, R.; López-Jurado, J.L.; Serra, M.; Zunino, P.; Pascual, J.; Salat, J. Updating temperature and salinity mean values and trends in the Western Mediterranean: The RADMED project. *Prog. Oceanogr.* **2017**, *157*, 27–46. [[CrossRef](#)]
72. Leaman, K.D.; Schoot, F.A. Hydrographic Structure of the Convection Regime in the Gulf of Lions: Winter 1987. *J. Phys. Oceanogr.* **1991**, *21*, 575–598. [[CrossRef](#)]
73. López-Jurado, J.L.; González-Pola, C.; Vélez-Belchí, P. Observation of an abrupt disruption of the long-term warming trend at the Balearic Sea, western Mediterranean Sea, in summer 2005. *Geophys. Res. Lett.* **2005**, *32*, L24606. [[CrossRef](#)]
74. Rohling, E.J.; Bryden, H.L. Man-induced salinity and temperature increases in the Western Mediterranean Deep Water. *J. Geophys. Res.* **1992**, *97*, 11191–11198. [[CrossRef](#)]

75. Béthoux, J.P.; Gentili, B. The Mediterranean Sea, coastal and deep-sea signatures of climatic and environmental changes. *J. Mar. Syst.* **1996**, *7*, 383–394. [[CrossRef](#)]
76. Smith, R.O.; Bryden, H.L.; Stansfield, K. Observations of new western Mediterranean deep water formation using Argo floats 2004–2006. *Ocean. Sci.* **2008**, *4*, 133–149. [[CrossRef](#)]
77. Grignon, L.; Smeed, D.A.; Bryden, H.L.; Schroeder, K. Importance of the variability of hydrographic preconditioning for deep convection in the Gulf of Lion, NW Mediterranean. *Ocean. Sci.* **2010**, *6*, 573–586. [[CrossRef](#)]
78. Schröder, K.; Gasparini, G.P.; Tangherlini, M.; Astraldi, M. Deep and intermediate water in the western Mediterranean under the influence of the Eastern Mediterranean Transient. *Geophys. Res. Lett.* **2006**, *33*, L21607. [[CrossRef](#)]
79. Marty, J.C.; Chiavérini, J. Hydrological changes in the Ligurian Sea (NW Mediterranean, DYFAMED site) during 1995–2007 and biogeochemical consequences. *Biogeosciences* **2010**, *7*, 2117–2128. [[CrossRef](#)]
80. Houpert, L.; Durrieu de Madron, X.; Testor, P.; Bosse, A.; D’Ortenzio, F.; Bouin, M.N.; Dausse, D.; Le Goff, H.; Kunesch, S.; Labaste, M.; et al. Observations of open-ocean deep convection in the northwestern Mediterranean Sea: Seasonal and interannual variability of mixing and deep water masses for the 2007–2013 Period. *J. Geophys. Res. Ocean.* **2016**, *121*, 8139–8171. [[CrossRef](#)]
81. Fuda, J.L.; Etiope, G.; Millot, C.; Favali, P.; Calcara, M.; Smriglio, G.; Boschi, E. Warming, salting and origin of the Tyrrhenian Deep Water. *Geophys. Res. Lett.* **2002**, *29*, 1898. [[CrossRef](#)]
82. Zunino, P.; Vargas-Yárñez, M.; Moya, F.; García-Martínez, M.C.; Plaza, F. Deep and intermediate layer warming in the western Mediterranean: Water mass changes and heaving. *Geophys. Res. Lett.* **2009**, *36*, L20608. [[CrossRef](#)]
83. Ozer, T.; Gertman, I.; Kress, N.; Silverman, J.; Herut, B. Interannual thermohaline (1979–2014) and nutrient (2002–2014) dynamics in the Levantine surface and intermediate water masses, SE Mediterranean Sea. *Glob. Planet. Chang.* **2017**, *151*, 60–67. [[CrossRef](#)]